Published in final edited form as:
Biochem Biophys Res Commun. 2011 July 29; 411(2): 323–328. doi:10.1016/j.bbrc.2011.06.140.

FBN1 isoform expression varies in a tissue and development-specific fashion

Mary E. Burchett[1], **I-Fang Ling**[2], and **Steven Estus**[2,*]

Mary E. Burchett: mary.burchett@uky.edu; I-Fang Ling: ifang.ling@gmail.com; Steven Estus: steve.estus@uky.edu

[1]University of Kentucky College of Medicine, University of Kentucky, Lexington, KY

[2]Department of Physiology, Sanders-Brown Center on Aging, University of Kentucky, Lexington, KY

Abstract

Mutations in *FBN1* cause Marfan syndrome, a heritable disorder of connective tissue. *FBN1* encodes the extracellular matrix protein, fibrillin. Our objective was to elucidate the extent that variation in RNA splicing contributes to *FBN1* isoforms. To identify *FBN1* splice variants, we scanned each of its 64 internal exons in a set of pooled human brain cDNA samples. *FBN1* splicing is generally efficient as we identified only two variants. Neither variant has previously been reported in the literature and include (i) an isoform which contains a cryptic 105 basepair exon between exons 54–55 (*54A-FBN1*) and (ii) an isoform which contains a cryptic 62 basepair exon between exons 57 and 58 (*57A-FBN1*). We compared *57A-FBN1* and *FBN1* expression in multiple human tissues, including adult skeletal muscle and brain, as well as fetal skeletal muscle, brain, liver, aorta, lung, skin, and heart. *57A-FBN1* represents 8–44% of *FBN1* mRNA and varies in a tissue- and development-specific fashion. In adult brain, *57A-FBN1* represented 39 ± 3 (%, mean ± SD) of total *FBN1* expression. In contrast, *57A-FBN1* represented 19 ± 2 (%, mean ± SD) of *FBN1* expression in skeletal muscle. In fetal tissue, the *57A-FBN1* proportion was highest in brain (27%) and low elsewhere, e.g., skin, aorta and lung (9–13%). In summary, a significant proportion of *FBN1* is expressed as *57A-FBN1* and this proportion varies in a tissue- and development-specific fashion. Since the 57A insertion creates a premature stop codon that mimics Marfan-associated mutations, the protein encoded by *57A-FBN1* is likely to not be functional. These results suggest that altered splicing may modulate disease severity, regulate *FBN1* expression, and potentially represent a therapeutic target.

Keywords

(6) Marfan syndrome; fibrillin; alternative splicing; isoforms

1. Introduction

Mutations in *FBN1* cause Marfan syndrome, a heritable disorder of connective tissue. *FBN1* encodes the extracellular matrix protein, fibrillin [1]. In the extracellular matrix, fibrillin acts

*-to whom correspondence can be addressed: Steven Estus, Phone: (859) 323-3985, ext. 264, Fax: (859) 323-2866, steve.estus@uky.edu, 800 S. Limestone St., Lexington, KY 40536-0230.

as a reservoir for transforming growth factor-β (TGF-β). Decreased deposition of fibrillin in the extracellular matrix leads to enhanced TGF- β signaling and the resultant Marfan phenotype (reviewed in [2]). *FBN1* expression is widespread based upon *in situ* hybridization and immunocytochemistry [3, 4].

Variation in RNA splicing is emerging as a mechanism that modulates disease susceptibility and severity (reviewed in [5, 6]). This emergence has lead to a nascent pharmacological approach to ameliorate disease phenotypes by using small molecules to alter splicing (reviewed in [7]). Here, we test the hypothesis that atypical *FBN1* splicing represents a significant proportion of *FBN1* expression. We identify two previously unreported *FBN1* splice variants that incorporate cryptic exons from introns 54 and 57 (designated *54A-FBN1* and *57A-FBN1*, respectively). Moreover, we show that *57A-FBN1* expression varies among tissues and between the fetal and adult stages. Since *57A-FBN1* expression ranges from 10–40% of total *FBN1* expression and the protein encoded by *57A-FBN1* is similar to that associated with a Marfan-associated mutation, decreasing *57A-FBN1* as a proportion of *FBN1* expression may offer a future therapeutic approach.

2. Materials and Methods

2A. Human tissue

The human brain and liver samples used for this study have been described in detail elsewhere [8, 9, 10, 11]. Briefly, the brain samples were obtained from the University of Kentucky Alzheimers Center while the liver samples were obtained from the Brain and Tissue Bank for Developmental Disorders in Baltimore, MD. The brain and liver samples were from deceased individuals with an average age at death of 83 years (range of 68–105) and 27 years (range of 13–46), respectively. Skeletal muscle samples were also obtained from the Brain and Tissue Bank for Developmental Disorders and were from deceased male individuals with an average age at death of 38 years (range of 20–61). Total RNA from human fetal skeletal muscle, brain, liver, aorta, lung, skin, and heart was obtained from Stratagene. Gestational ages ranged from 16–22 weeks.

2B. Cell Culture

HepG2 (human hepatocellular carcinoma), SH-SY5Y (human neuroblastoma), HEK293 (human embryonic kidney), H4 (human neuroglioma), and MCF-7 (human breast adenocarcinoma) cell lines were maintained in Dulbecoo's modified Eagle's medium (DMEM) supplemented with 10% fetal bovine serum and 50 U/ml penicillin and 50 μg/ml streptomycin at 37°C in a humidified 5% CO_2-95% air atmosphere.

2C. PCR Amplification

RNA was extracted and converted to cDNA in one microgram aliquots using SuperScriptIII reverse transcriptase (Invitrogen) and random hexamers (Invitrogen) as described previously [8, 10, 12]. Primer pairs were designed to produce overlapping products; this enabled evaluation of splicing efficiency of each internal exon (Table 1). These primer pairs were then used to screen for splice variants in cDNA pooled from 20 brain samples. The pooled cDNA was amplified with each primer pair by using Platinum Taq (Invitrogen) and cycling conditions of a pre-incubation for 3 minutes at 95° C, followed by 34 cycles of 94°C for 30 seconds, 60°C for 30 seconds, and 72°C for 60 seconds (Perkin Elmer 9600). PCR products were separated by electrophoresis in an 8% polyacrylamide gel, detected by SYBR-gold staining, and visualized by using a fluorescence imager (Fuji FLA-2000). PCR products that were different than the expected size were identified by direct sequencing (Davis Sequencing).

2D. Real-time PCR (RT-PCR)

The expression level of the *57A-FBN1* isoform, which contains a cryptic exon within intron 57, as well as the *FBN1* isoform without this cryptic exon (*FBN1*) were quantified by using RT-PCR. Each assay used a common antisense primer corresponding to sequence within exon 59, i.e., 5′-TTCGGCAAACATCGTGAATA-3′. The sense primer for *FBN1* detection corresponded to sequence within exon 57, i.e., 5′-CTTGACAATCGGGAAGGGTA-3′ while the sense primer for *57A-FBN1* quantification corresponded to sequence within exon 57A, i.e., 5′-ACCCAGGACAATCGGGAAG-3′. The 20 μl reaction mixture, which contained 20 ng of cDNA, 1 μM of each primer and 1× PerfecTaqPCR Supermix (Quanta Biosciences, Gaithersburg, MD) was subjected to RT-PCR (MJ Research PTC-200 with Chromo4 detector) with conditions of a preincubation at 95°C for 120 seconds, followed by 40 cycles of 95°C for 15 seconds, 60°C for 30 seconds, and 72°C for 20 seconds. Reaction specificity was evaluated by subjecting the PCR products to gel electrophoresis and by performing a melting curve analysis after PCR amplification. The copy numbers of PCR product in each sample were determined relative to standard curves that were amplified in parallel and were based upon purified and quantified PCR products. For the brain and fetal tissue RNAs, copy numbers were then normalized to the geometric mean of the copy numbers of hypoxanthine-guanine phosphoribosyltransferase 1 (HPRT) and ribosomal protein L32 (RPL32) as previously described [13]. Since the hypoxanthine-guanine phosphoribosyltransferase 1 and ribosomal protein L32 geometric mean showed unacceptable variation among the adult skeletal muscle samples, the expression of *FBN1* in these samples was normalized to the *18S rRNA* copy number. All real-time PCR assays were repeated twice.

3. Results

3A. Identification of *FBN1* Splice Variants

To detect alternatively spliced *FBN1* exons, we scanned the 64 internal exons of *FBN1* in human brain cDNA for inefficient splicing or the presence of cryptic exons. *FBN1* exons were generally spliced efficiently because a single PCR product of the expected size was produced in most reactions (Figure 1A). However, several PCR reactions amplified two products that sequencing established as representing *FBN1* splice variants. In particular, sequencing of the PCR products generated from exons 50–55 and from 54–58 revealed the expected isoform as well as a novel isoform that includes a cryptic 105 bp exon from within intron 54. This 105 bp exon is predicted to introduce a premature stop codon, resulting in a truncated fibrillin protein of 2,217 amino acids as compared to the standard 2,871 amino acid fibrillin (Figure 1B). Sequencing of the PCR products amplified between exons 57–61 revealed the expected isoform, which contained exons 57–61, as well as an isoform which contained a 62 bp cryptic exon from intron 57; this isoform has not been reported in the literature but is in the Ensembl database (http://uswest.ensembl.org/Homo_sapiens/Transcript/Summary?db=core;g=ENSG00000166147;r=15:48700505-48937918;t=ENST00000389087). The insertion of exon 57A is predicted to cause a frameshift and subsequent premature termination codon, producing a truncated 2,417 amino acid fibrillin (Figure 1C). Since the standard 2,871 amino acid fibrillin polymerizes in a head-to-tail fashion in the extracellular matrix [14], the truncated proteins encoded by *54A-FBN1* and *57A-FBN1* may disrupt the structure of fibrillin in the extracellular matrix.

3B. Comparison of *57A-FBN1* between individuals and tissues

To investigate expression of these isoforms, we focused upon the *57A-FBN1* prototypic isoform because of its prior listing in Ensembl. When we quantified the expression of *57A-FBN1* and *FBN1* in a series of 34 brain samples by quantitative RT-PCR, we found that

57A-FBN1 was expressed consistently among individual samples and accounted for 39 ± 3 (%, mean ±SD, n=34, Figure 2A–B) of total *FBN1* expression. Hence, *57A-FBN1* represents a major *FBN1* isoform in the brain. We next compared the expression of *FBN1* and *57A-FBN1* in a series of adult skeletal muscle samples, a tissue in which Marfan pathology is observed. When we compared across the cohort, we found that *57A-FBN1* represented a consistent 19 ± 2 (%, mean ±SD, n=9, Figure 2C–D) of total *FBN1* mRNA. Hence, the proportion of *57A-FBN1* in adult tissues varies strikingly between tissues but varies little between individuals.

Since *FBN1* mutations alter tissue formation during development, especially in the fetal aorta, skeletal muscle, heart, lung and skin (reviewed in [15, 16]), we proceeded to compare *FBN1* and *57A-FBN1* in these fetal tissues as well as fetal brain, liver and kidney (Figure 3A–B). We found that the proportion of *57A-FBN1* was highest in the fetal brain and relatively uniform in aorta, heart, lung, liver, kidney, skeletal muscle and skin (Figure 3A). Furthermore, total *FBN1* expression was highest in skin, moderate in aorta, heart, lung, kidney, and skeletal muscle, and low in brain and liver (Figure 3B). Interestingly, this pattern of *FBN1* expression recapitulates the phenotype of Marfan syndrome in that tissues with higher total *FBN1* expression, i.e., skin, aorta, heart, lung and skeletal muscle, generally have significant pathology in Marfan syndrome relative to two tissues with low expression, brain and liver [15, 16]. Since *FBN1* function is often studied in cell lines [17], we also investigated the proportion of *57A-FBN1* in several cell lines. The proportion of *57A-FBN1* ranged from 9–15% of total *FBN1* expression (Figure 3C), which was similar to the proportion of *57A-FBN1* in the majority of fetal tissues examined. *FBN1* expression was low in these cell lines, relative to the fetal tissues, with H4 neuroglioma cells being highest and human embryonic kidney (HEK) 293 and MCF-7 breast cancer cells being lowest (Figure 3D).

4. Discussion

Our primary findings are that (i) the exons of *FBN1* are generally spliced with high efficiency, (ii) two *FBN1* isoforms not previously described in the literature are generated by the inclusion of cryptic exons from introns 54 and 57 and (iii) the quantities of one isoform, *57A-FBN1*, are sufficiently large to account for a significant proportion of *FBN1* expression. Moreover, the proportion of *FBN1* expression as *57A-FBN1* varies in a tissue- and development-specific fashion. If the fibrillin variant protein encoded by *57A-FBN1* is not functional, optimizing *FBN1* splicing to minimize *57A-FBN1* may represent a therapeutic approach to ameliorate the Marfan syndrome phenotype.

Although the functional impact of *FBN1* truncation after exons 54 or 57 is unclear, *in vivo* and *in vitro* evidence suggests that these truncated fibrillin proteins will not be functional. First, at the human level, many mutations that cause Marfan syndrome are the result of similarly truncated fibrillin proteins (FBN1 mutation list can be found at http://www.umd.be:2030/W_FBN1/indexR_FBN1.shtml). For example, a single basepair deletion within exon 57 (at amino acid 2347) and the resulting frameshift and stop codon eighteen amino acids later, causes Marfan syndrome [18]. Second, *in vitro* studies have found that the portion of fibrillin encoded after exon 62 is necessary for fibrillin multimerization [14]. Hence, the truncated proteins encoded by *54A-FBN1* and *57A-FBN1* are highly likely to be nonfunctional. Individuals with a greater proportion of *57A-FBN1* due to variation in splicing would be predicted to have a more severe Marfan syndrome phenotype (Figure 4) because lower fibrillin protein results in greater TGF-β signaling. Hence, variations in *FBN1* splicing may offer one possible mechanism for the intra-familial variability seen in people with Marfan syndrome.

Nonsense mediated decay (NMD) has been reported to degrade some abnormally spliced *FBN1* variants, including a variant wherein exon 51 is skipped [19]. Whether NMD regulates the levels of *54A-FBN1* or *57A-FBN1* is unclear. We interpret the finding that *57A-FBN1* represents 10–40% of *FBN1* mRNA as suggesting that at least *57A-FBN1* is likely not subjected to NMD; the alternative interpretation would require that *57A-FBN1* represents the major *FBN1* isoform prior to NMD for 10–40% of *FBN1* to be present as *57A-FBN1* after NMD. Alternatively, if *57A-FBN1* does undergo NMD, expression of the *57A-FBN1* variant and subsequent NMD may represent a mechanism regulating total *FBN1* expression. In this event, identifying splicing regulatory proteins that minimize exon 57A inclusion may be an especially robust means to enhance *FBN1* expression.

In summation, *FBN1* exons are generally included with high efficiency in mature *FBN1*. However, we have identified two previously unreported *FBN1* isoforms, and note that one isoform, *57A-FBN1*, represents a significant portion of total *FBN1* expression. Since the protein encoded by *57A-FBN1* is likely to be non-functional, efforts to decrease the proportion of *FBN1* expressed as *57A-FBN1* represents a potential therapeutic modality.

Acknowledgments

The authors gratefully acknowledge tissue supplied by the University of Kentucky Alzheimers Disease Center, which is supported by P30AG028383, NIH for grant support (R01AG026147 and P01AG030128), and Dr. Hal Dietz (Johns Hopkins University) for helpful discussion.

Abbreviations

RT-PCR	Real-time PCR
HEK	human embryonic kidney
NMD	Nonsense mediated decay

References

1. Dietz HC, Cutting GR, Pyeritz RE, Maslen CL, Sakai LY, Corson GM, Puffenberger EG, Hamosh A, Nanthakumar EJ, Curristin SM, et al. Marfan syndrome caused by a recurrent de novo missense mutation in the fibrillin gene. Nature. 1991; 352:337–9. [PubMed: 1852208]
2. Dietz HC. TGF-beta in the pathogenesis and prevention of disease: a matter of aneurysmic proportions. J Clin Invest. 2010; 120:403–7. [PubMed: 20101091]
3. Zhang H, Hu W, Ramirez F. Developmental expression of fibrillin genes suggests heterogeneity of extracellular microfibrils. J Cell Biol. 1995; 129:1165–76. [PubMed: 7744963]
4. Quondamatteo F, Reinhardt DP, Charbonneau NL, Pophal G, Sakai LY, Herken R. Fibrillin-1 and fibrillin-2 in human embryonic and early fetal development. Matrix Biol. 2002; 21:637–46. [PubMed: 12524050]
5. Ward AJ, Cooper TA. The pathobiology of splicing. J Pathol. 2010; 220:152–63. [PubMed: 19918805]
6. Poulos MG, Batra R, Charizanis K, Swanson MS. Developments in RNA Splicing and Disease. Cold Spring Harb Perspect Biol. 2010
7. Dietz HC. New therapeutic approaches to mendelian disorders. N Engl J Med. 2010; 363:852–63. [PubMed: 20818846]
8. Zhu H, Tucker HM, Grear KE, Simpson JF, Manning AK, Cupples LA, Estus S. A common polymorphism decreases low-density lipoprotein receptor exon 12 splicing efficiency and associates with increased cholesterol. Hum Mol Genet. 2007; 16:1765–72. [PubMed: 17517690]
9. Zou F, Gopalraj RK, Lok J, Zhu H, Ling IF, Simpson JF, Tucker HM, Kelly JF, Younkin SG, Dickson DW, Petersen RC, Graff-Radford NR, Bennett DA, Crook JE, Estus S. Sex-dependent association of a common low-density lipoprotein receptor polymorphism with RNA splicing

efficiency in the brain and Alzheimer's disease. Hum Mol Genet. 2008; 17:929–35. [PubMed: 18065781]

10. Grear KE, Ling IF, Simpson JF, Furman JL, Simmons CR, Peterson SL, Schmitt FA, Markesbery WR, Liu Q, Crook JE, Younkin SG, Bu G, Estus S. Expression of SORL1 and a novel SORL1 splice variant in normal and Alzheimers disease brain. Mol Neurodegener. 2009; 4:46. [PubMed: 19889229]
11. Ling IF, Estus S. Role of SFRS13A in low-density lipoprotein receptor splicing. Hum Mutat. 2010; 31:702–9. [PubMed: 20232416]
12. Chomczynski P, Sacchi N. Single-step method of RNA isolation by acid guanidinium thiocynate-phenol-chloroform extraction. Anal Biochem. 1987; 162:156–159. [PubMed: 2440339]
13. Vandesompele J, De Preter K, Pattyn F, Poppe B, Van Roy N, De Paepe A, Speleman F. Accurate normalization of real-time quantitative RT-PCR data by geometric averaging of multiple internal control genes. Genome Biol. 2002; 3:RESEARCH0034. [PubMed: 12184808]
14. Hubmacher D, El-Hallous EI, Nelea V, Kaartinen MT, Lee ER, Reinhardt DP. Biogenesis of extracellular microfibrils: Multimerization of the fibrillin-1 C terminus into bead-like structures enables self-assembly. Proc Natl Acad Sci U S A. 2008; 105:6548–53. [PubMed: 18448684]
15. Ramirez F, Dietz HC. Marfan syndrome: from molecular pathogenesis to clinical treatment. Curr Opin Genet Dev. 2007; 17:252–8. [PubMed: 17467262]
16. Judge DP, Dietz HC. Marfan's syndrome. Lancet. 2005; 366:1965–76. [PubMed: 16325700]
17. Summers KM, Bokil NJ, Baisden JM, West MJ, Sweet MJ, Raggatt LJ, Hume DA. Experimental and bioinformatic characterisation of the promoter region of the Marfan syndrome gene, *FBN1*. Genomics. 2009; 94:233–40. [PubMed: 19573590]
18. Korkko J, Kaitila I, Lonnqvist L, Peltonen L, Ala-Kokko L. Sensitivity of conformation sensitive gel electrophoresis in detecting mutations in Marfan syndrome and related conditions. J Med Genet. 2002; 39:34–41. [PubMed: 11826022]
19. Dietz HC, Kendzior RJ Jr. Maintenance of an open reading frame as an additional level of scrutiny during splice site selection. Nat Genet. 1994; 8:183–8. [PubMed: 7842017]

Highlights

- We evaluate splicing in *FBN1*, mutations in which cause Marfan syndrome.
- We report two *FBN1* splice variants that are both predicted to produce non-functional protein.
- The expression of one isoform, *57A-FBN1*, varies between tissues and with development.
- *57A-FBN1* represents a significant proportion of *FBN1* expression.
- *57A-FBN1* may regulate fibrillin expression and disease severity.

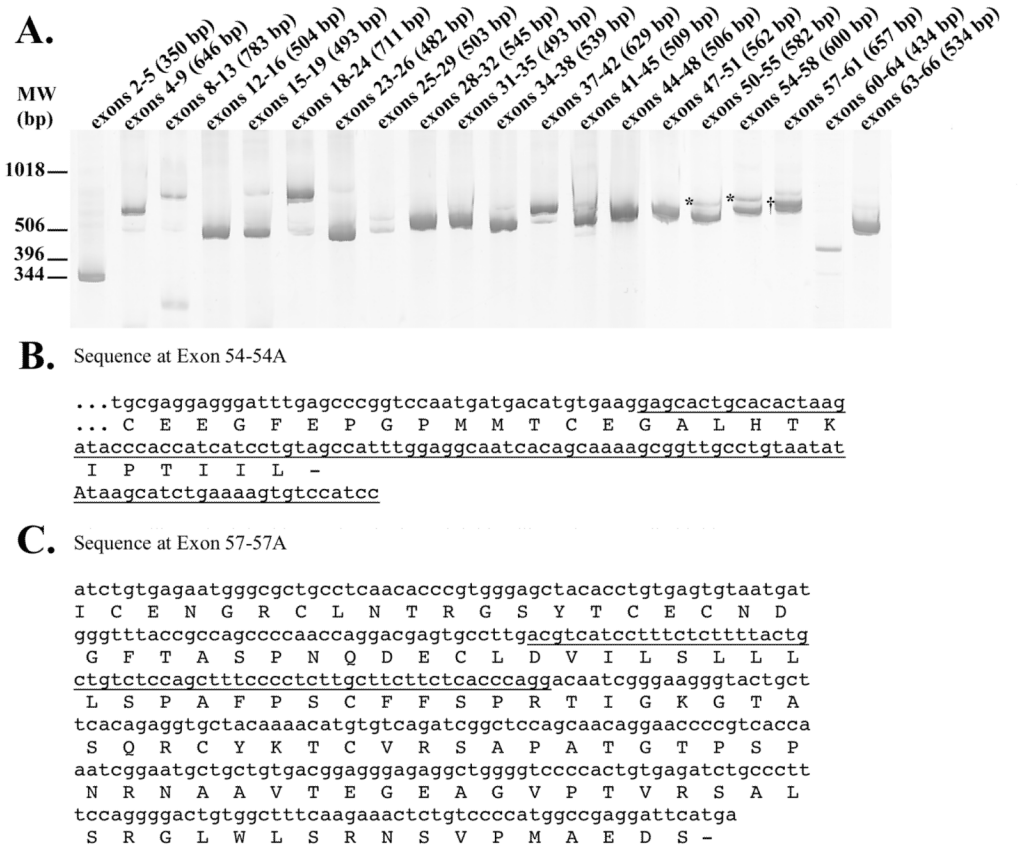

Figure 1. *FBN1* Splicing Patterns in Human Brain Tissue

The products of PCR amplification of human brain cDNA across the indicated exons were separated by polyacrylamide gel electorphoresis and visualized by SYBR gold fluorescence; the sizes of the expected products are shown in parentheses (A). Since this is a composite image of multiple gels, the molecular weight markers are approximate. The nucleotide and protein sequence corresponding to the products marked with an * show that retention of a cryptic exon within intron 54 (underlined) introduces a premature translation termination codon (B). Similarly, the nucleotide and predicted protein sequence of the PCR product marked with a † shows retention of a cryptic exon within intron 57 (underlined) that causes a frameshift and premature termination codon (C).

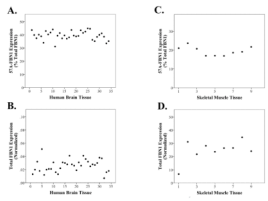

Figure 2. Quantitation of *57A-FBN1* and Total *FBN1* in Human Adult Tissue

Real time PCR quantification of *57A-FBN1* and *FBN1* shows that *57A-FBN1* represents a consistent proportion of total *FBN1* expression in brain (A–B) and skeletal muscle (C–D). A greater proportion of FBN1 is expressed as *57A-FBN1* in the brain. Each data point represents a single human sample analyzed. Since *HPRT* and *RPL32* were not consistent in the muscle samples, FBN1 expression was normalized to *18S rRNA* in the muscle samples.

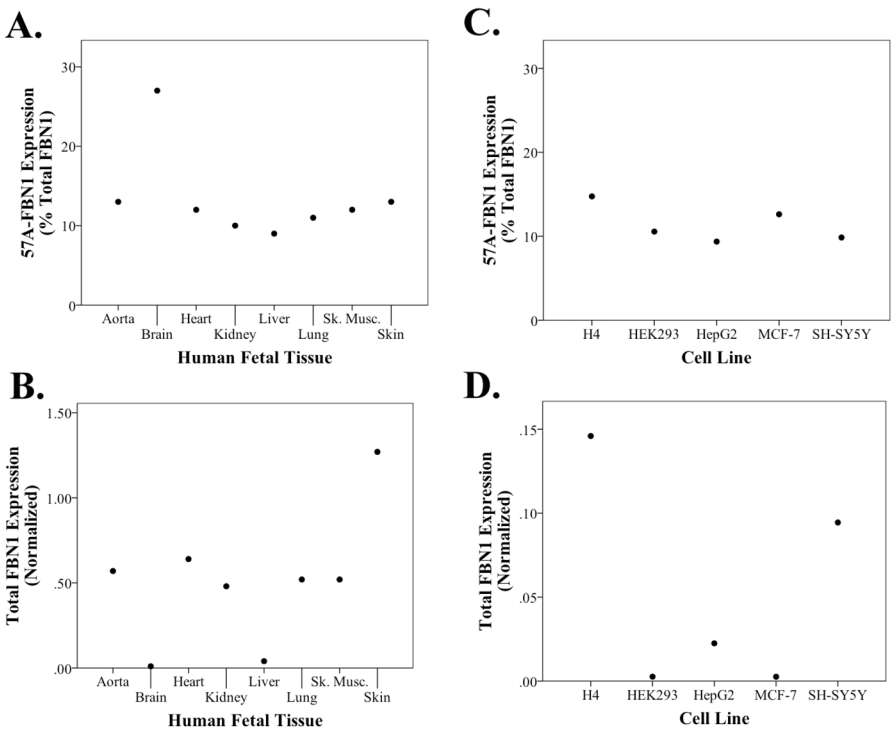

Figure 3. Quantitation of *57A-FBN1* and Total *FBN1* in Embryonic Human Tissues and Commonly Used Human Cell Lines

Real time PCR quantification shows that *57A-FBN1* represents a consistent ~12% (A, C) of total *FBN1* expression (B, D) across a series of human embryonic tissues and cell lines, with the exception of brain tissue, which has a higher proportion of *57A-FBN1*.

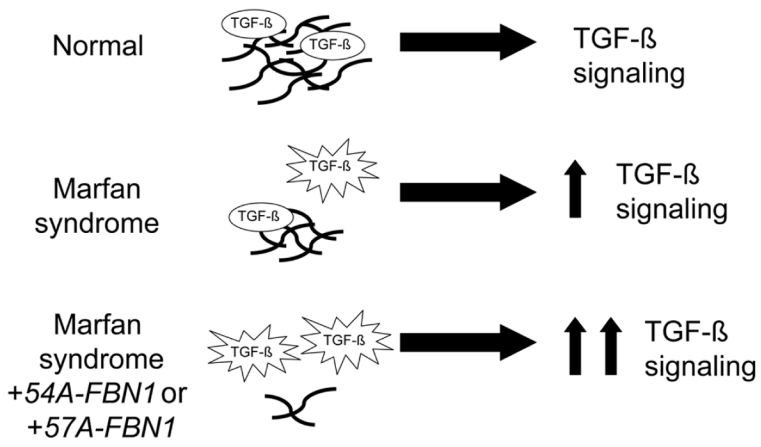

Figure 4. Model for *FBN1* Isoforms in Marfan Syndrome

Fibrillin polymers (black lines) in the extracellular matrix serve to maintain a TGF-β reservoir. In Marfan syndrome, a decrease in fibrillin polymer results in increased TGF-β signaling and the Marfan phenotype. The two isoforms identified here are predicted to produce truncated fibrillin proteins that mimic the effects of Marfan-associated mutations. Hence, these isoforms are likely to exacerbate Marfan syndrome.

Table 1

PCR primers.

Exon Amplified	Primer	Primer Sequence
2–5	2F	CCGTGCTTTTAGCGTCCTAC
	5R	ACTGCAGCTACCTCCATTCA
4–9	4F	CTGTGGGGATGGATTTTGTT
	9R	TTCACCCCCTTCACAGATTC
8–13	8F	GGCTCTGTCAGGGAGGAAAT
	13R	GGCACTGACAGGTGTACGAA
12–16	12F	AGTGCAACAAAGGGTTCCAG
	16R	GTCCAGGGAAGCATTCACAT
15–19	15F	TGGATGAATGCAGCATAAGG
	19R	CCATTTGGGCAAATATCAGG
18–24	18F	CGGAATATCAGGCACTCTGC
	24R	TCATTCCACTGGGACACTGA
23–26	23F	TCCCATATGTGGTAAAGGGTACT
	26R	TGCACTTAAAGCTGCCAATG
25–29	25F	CTGGAAACCTGCTTCCTGAG
	29R	TCCTCGCATTCCTCAGTACC
28–32	28F	ATCCTCTCCTATGCCGAGGT
	32R	GCCTTTCGTGTTTTCACAGG
31–35	31F	TGGATTCATGGCATCTGAAG
	35R	GCATTCACAGCGGTATCCTC
34–38	34F	CATGGGATCTTACCGCTGTC
	38R	AGCAGGAAGCTTTGGAAACA
37–42	37F	GTGACTGCCCACCTGATTTT
	42R	GCAGCACATCTTCTTGGTCA
41–45	41F	TGTGGTCCAGGGACATGTTA
	45R	GTAGCTGCCTGCAGTGTTGA
44–48	44F	AGCTTCCGATGTGAATGTCC
	48R	CACTGGAAAGACCCCACTGT
47–51	47F	AAGAGATGCCTGTGGGAATG
	51R	GCATTCCTGCTTGGAGTGAT
50–55	50F	CTGGGCACATGCAGTAACAC
	55R	GAAGGCACAGAGCAGAGGAT
54–58	54F	CCTGCAAGAATGTGATTGGA
	58R	AAGGGCAGATCTCACAGTGG
57–61	57F	AAGCCAGGGATCTGTGAGAA
	61R	GGTAAATCCGGGAGGACATT
60–64	60F	TCCCAAACCCTGCAATTTTA
	64R	CGGGACACATGCACTTGTAG
63–66	63F	ATGGCTGCCAGAACATCATT

Exon Amplified	Primer	Primer Sequence
	66R	CCCAACTTGCAAGACTCACA